International Journal of Engineering Research & Technology (IJERT)
ISSN: 2278-0181
Vol. 4 Issue 07, July-2015

Crystalization, Spectroscopic and Optical Investigation of Potassium Hydrogenselenate ($KHSeO_4$) Single Crystals

A. Abu El-Fadl*
Physics Department, Faculty of Science
Assiut University
Assiut, Egypt

A. M. Nashaat
Physics Department, Faculty of Science
Assiut University
Assiut, Egypt

Abstract: **Single crystals of potassium hydrogenselenate were successfully grown by solution growth technique. The presence of functional groups in the crystal lattice was qualitatively analyzed by FTIR spectrum The optical absorption spectra were recorded for $KHSeO_4$ single crystals along the a-, b-, and c-axes.. The dependence of the absorption coefficient (α) on the photon energy (hν) was determined for the principal axes and the crystals show indirect allowed inter-band transitions. The absorption coefficient (α), indirect optical energy gap (E_g), extinction coefficient (k), refractive index (n) and related parameters were found to be dependent on the measured axis. To explain the dispersion of the refractive index in the principal crystal axes the single oscillator model by Wemple-DiDomenico was used and the dispersion parameters were calculated.**

Keywords; $KHSeO_4$ single crystals, FTIR Spectroscopy, Optical energy gap, Dispersion parameters, Optical constants.

1. Introduction

$MHXO_4$ crystals (M=K, Rb, Cs and NH_4, X=S or Se) has been widely studied because of its high proton conductivity, its phase transition behavior and the possible usage in fuel cells [1]. These crystals show various possible applications by changing alkaline metal site M and some of these crystals exhibit ferroelectric properties [2]. One member of the $MHXO_4$ crystal family is the potassium hydrogenselenate ($KHSeO_4$) crystal, which crystallizes in the orthorhombic system with Pbca space group [3]. The most interesting group in this crystal structure is the hydrogen selenite ($HSeO_4$) ion, which is usually found to be distorted and arranged in a tetrahedral ions, these ions are connected to each other with short hydrogen bonds. Therefore, the crystal structure of $KHSeO_4$ crystal contains simultaneously infinite chains and cyclic dimers of the hydrogen-bonded $HSeO_4$ anions [3].

FTIR spectroscopy of a compound provides more information than normally available electronic spectra. The presence or absence of absorption bands helps in predicting the presence of functional groups in the compound.

The investigation of the fundamental absorption edge can provide extensive information about the band structure of crystals, disorder effects, the character of electron–phonon interaction and existence of exciton and their role in the absorption mechanism. This can provide also information about the mechanism of the optical transition.

Optical constants define how light interacts with a material. The determination of these optical constants is expected to provide more physical information about the spectral dependence of optical parameters (such as refractive index, extinction coefficient, real and imaginary dielectric constant and absorption coefficients) which are essential in characterizing materials used in the fabrication of optoelectronic devices [4].

Our goal in this study is to investigate the optical parameters for $KHSeO_4$ crystal along the a-, b- and c-axes and explain the dispersion of the refractive index in terms of the Wemple-DiDomenico single-effective-oscillator model. Another goal is to study the vibration bands for this crystal by Fourier transform infrared (FTIR) spectroscopy.

2. Experimental

Saturated solutions of H_2SeO_4 mixed with K_2SeO_4 were prepared. The obtained solution was allowed to evaporate at room temperature by conventional isothermal method. Crystals up to 2 to 3 mm in dimensions could be grown over the period of 72 hours. Best crystals were collected and used as seed crystals. 250 ml of saturated solutions were taken in the crystal growth apparatus fabricated in our laboratory and placed on the platform of a constant temperature bath with an accuracy of ±0.1°C and was allowed to equilibrate at 45°C. Optically good quality seed crystals were suspended firmly inside the solutions using a nylon thread. The jars containing the solution were covered by a transparent polythene sheet to prevent the evaporation of the solvent. The growth runs were initiated by reducing the temperature at the rate of 0.2°C/day. After several weeks, the solutions lead to nearly perfect single crystals. Their chemical syntheses are reproducible, and the crystals obtained in this way are pure, having appropriate sizes and stable under normal conditions of temperature and humidity. The formula of this material was determined by chemical analysis and confirmed by structural refinement.

NICOLET FTIR 6700 spectrometer was used to record the FTIR spectra in the range 400 - 4000 cm^{-1} by the KBr pellet method to study the functional groups of the samples.

The grown crystal was cut into thin plates along the a-, b- and c-axes. The plates were transparent and clear from any noticeable defects. Optical transmittance (T) and reflectance (R) were recorded at room temperature using Shimaduzu UV-VIS-2101 PC dual beam scanning spectrophotometer in the energy range 2.1-6.4 eV. The incident unpolarized light was nearly perpendicular to (100), (010) and (001) crystal planes.

3. Results and Discussion

3.1. Fourier Transform Infrared Spectroscopy

The spectra carried out in the range 400-4000 cm^{-1} of as grown $KHSeO_4$ crystals and crystal annealed for 1 and 2 hours at 150 °C as shown in Fig. 1 have been assigned in Table. 1 and all the peaks have been assigned to the corresponding functional groups. The peaks observed at the range (2923-1631) cm^{-1} are assigned to the symmetric vibration of O-H while the in-plane bending of O-H is assigned to the peaks observed in the wavenumber range (1424-1261) cm^{-1}. The symmetric and asymmetric vibrations of $Se-O_2$ are assigned to the peaks located at (965-914) and (884-877) cm^{-1}, respectively. Se-O-OH asymmetrical vibration is assigned to the peak observed near 825 cm^{-1}. SeO_4 symmetrical vibration and Se-OH symmetric vibration appear at 711 cm^{-1} and (421-404) cm^{-1} respectively. The peak appeared at 687.22 cm^{-1} with medium intensity is assigned to O-H degenerate deformation. The assignment of the functional groups is in good agreement with the literature [5, 6].

TABLE 1. Assignment of the FTIR absorption bands of $KHSeO_4$ single crystal.

Wavenumber (cm-1)			Assignment
As grown	Annealed at 150°C for 1h.	Annealed at 150°C for 2h.	
2923.54	2925.3	2923.62	O-H symmetric vibration
2452.88	2362.89	2453.91	
1631.66	1631.73	1631.59	
1424.37	1418.53	1424.6	O-H in-plane bending
1261	1261.36	1265.7	
956.74	956.77	965.81	$Se-O_2$ symmetric vibration
914.54	919.7	923.75	
884.13	883.55	877.39	$Se-O_2$ asymmetric vibration
825.12	825	826.16	Se-O-OH asymmetrical vibration
737.49	736.87		
711.29	711.03		Se-OH symmetric vibration
		687.22	O-H degenerate deformation
		553.84	
421.53	417.59	404.02	SeO_4 symmetrical vibration

The IR spectrum of heat treated samples (Fig. 1) indicated that there is no change in the frequency of most of the bands. A decrease in intensity of most bands has been recorded. Some sharp peaks become broad and some peaks almost vanished with increasing the annealing duration like the peaks around 737 cm^{-1}, 711 cm^{-1} and 421 cm^{-1} while peaks appeared stronger like the peaks centered at 1631.73 cm^{-1}, 687.22 cm^{-1} and 553.84 cm^{-1}. The broad hump near 3400 cm^{-1} increased in intensity with increasing the annealing duration and the small peaks near 2400 cm^{-1} decreased in intensity. The splitting in the peaks near 650 cm^{-1} decreased and the peaks begin to overlap. There is also a decrease in intensity of the peaks near 1300 cm^{-1}.

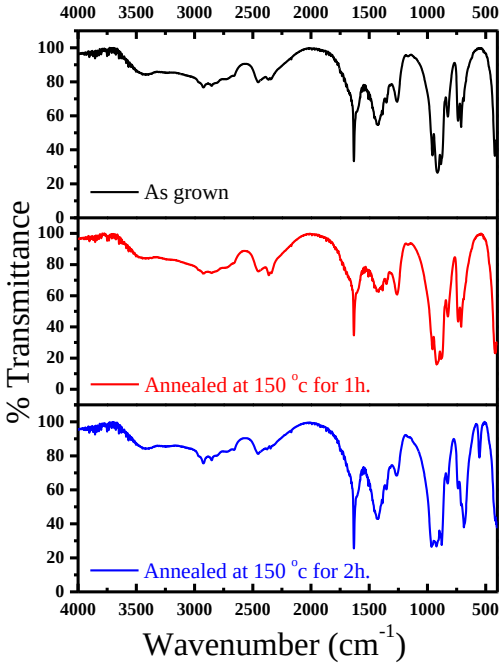

Fig. 1. *FTIR spectrum for as grown and annealed $KHSeO_4$ single crystals.*

3.2. *Optical absorption coefficient (α)*

The optical behavior of a material is generally utilized to determine its optical constants for example the absorption coefficient α. The absorption coefficient (α) spectra for different crystallographic axes are calculated from the transmittance data, the relation used is given by $\alpha = -(1/d)\ Ln\ T$, where d is the crystal thickness and T is the optical transmittance.

The spectral distribution of the absorption coefficient (α) for $KHSeO_4$ crystals along the principal crystallographic directions were plotted in the 4.0-5.4 eV portion of photon energy as shown in figure (Fig.2-i). It is observed that α is in continuous increasing with increasing hν, near the absorption edge α exhibits a steep rise and a straight line relationship is observed in the high region, it also shows that the magnitude of α and α–hν shape of the dependence at all energies are different for different crystal axis. On the other hand, its value for the b-axis is higher than that for the other two axes.

The optical absorption spectra reveal that no absorption peaks recorded in the range of photon energy (1.4- 6.5 eV) and the absence of absorption in the visible region clearly indicate that the grown crystal can be used for optoelectronic applications.

3.3. Optical band gap

The fundamental absorption edge is one of the most important features of the absorption spectrum of a material. The increased absorption near the edge is caused by the transition of electrons from the valence band to the conduction band. The optical band gap E_g of $KHSeO_4$ crystals can be determined from the dependence of absorption coefficient on the photon energy. The direct or indirect nature of optical transition between parabolic bands can be studied using the Tauc's expression [7]:

$$\alpha = \frac{B(h\nu - E_g)^r}{h\nu} \quad (1)$$

Where B is the proportionality factor and E_g is optical band-gap. Both values of B and E_g are constants or photon energy independent, the index r depends on the type of electronic transitions and assumes values of 1/2, 2, 3/2, and 3 for allowed direct, allowed indirect, forbidden direct and forbidden indirect transitions, respectively. For the $KHSeO_4$, value of r = 1/2 validates (1). A good fit of the experimental points with the above equation means that non-direct electronic transitions are the only mechanism responsible for the photon absorption inside $KHSeO_4$ crystals.

The values of $(\alpha h\nu)^{1/2}$ were calculated and plotted against hν. Fig. 2-ii shows a typical Tauc's plot. The straight portion of the curve was then extrapolated and its intersection on the abscissa was determined as shown in the inset of Fig. 2-ii. This value corresponds to the energy gap (E_g). Table 2 contains the data of optical band gap (E_g) which represents that, the value of E_g for the c-axis is greater than its value for the other two axes while the spectra of $(\alpha h\nu)^{1/2}$ preserves the same behavior as that of the absorption coefficient α.

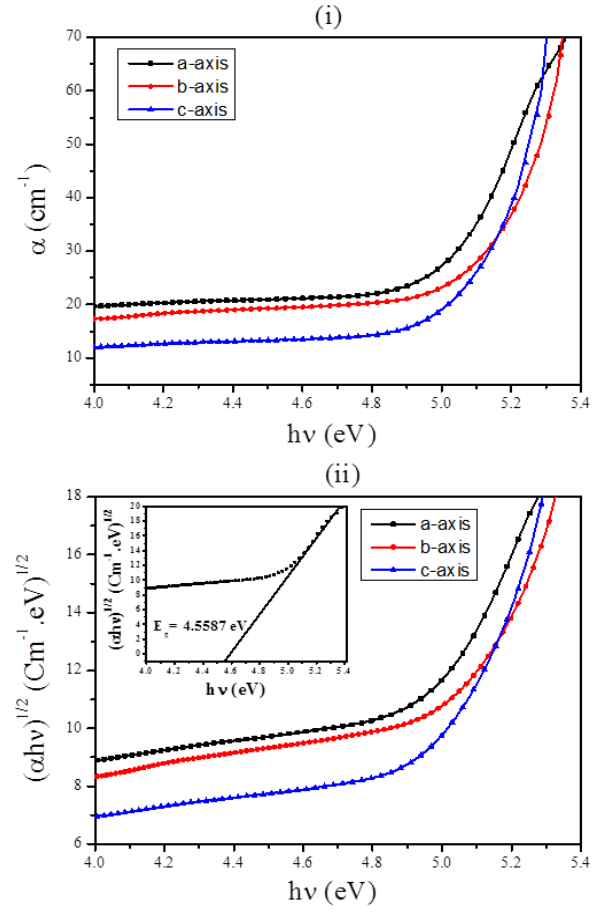

Fig. 2. The spectra of (i) absorption coefficient α and (ii) $(\alpha h\nu)^{1/2}$ with respect to the principle crystallographic axes of $KHSeO_4$ single crystal.

By tuning the optical energy gap (E_g) and tailoring the absorption coefficient (α) of the materials, we can active the desired material which is suitable for the fabrication of various optoelectronic devise.

3.4. Real and imaginary parts of the refractive index

The refractive index is explained in terms of real and imaginary parts. The real part of the refractive index (n) or simply the refractive index which describes the oscillations of the incident radiation in the crystal, while the imaginary part (k) known as the extinction coefficient which describes the attenuation of the incident radiation as it propagates in the crystal. The values of (n) and (k) can be determined from the absorption coefficient α and reflection (R) spectra (figure of R spectra not included). The Reflectance of the surface (R) is the written in terms of refractive index (n) as [8]:

$$R = \frac{(n-1)^2 + k^2}{(n+1)^2 + k^2} \quad (2)$$

While the extinction coefficient k is related to the absorption coefficient α by:

$$k = \frac{\alpha\lambda}{4\pi} \quad (3)$$

The dependence of refractive index (n) on the photon energy is shown in Fig. 3-i and it is seen that the refractive index measured in the b-axis direction has higher values than those measured in the other crystallographic directions. Fig. 3-ii shows the plot of extinction coefficient (k) as a function of photon energy hν.

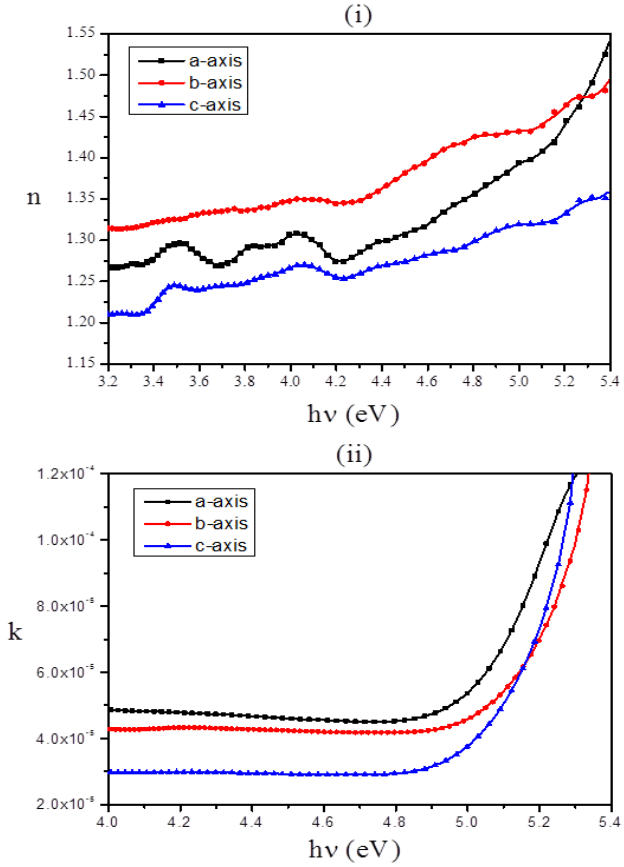

Fig. 3. The spectra of (i) refractive index n and (ii) extinction coefficient k with respect to the principle crystallographic axes of $KHSeO_4$ single crystal.

From the graph, it is clear that extinction coefficient (k) measured in the a-axis direction has higher values than those measured along the other two crystallographic directions unlike the refractive index which has higher values in the b-axis direction. Thus, the extinction coefficient (k) and refractive index (n) depend on the photon energy and the crystallographic direction. Fig. 3 may introduce that for this crystal the three crystallographic axes have different behaviors with the incident radiation as the radiation is attenuated most in the a-axis as indicated from the extinction coefficient values while the propagation of the incident radiation described by the refractive index is smoother in the b-axis direction.

It is understood that the higher value of photon energy will enhance the optical efficiency of the material. Hence, by tailoring the photon energy, one can achieve the desired material for optical device fabrication. Meanwhile the refractive index (n) and the extinction coefficient (k) are the basis for any optical constants.

3.5. Dispersion characterizations

To explain the dispersion of the refractive index of $KHSeO_4$ single crystal Wemple and DiDomenico (WDD) model is used which is based on single oscillator formula [9, 10]:

$$n^2(h\nu)-1=E_dE_{so}/[E_{so}^2-(h\nu)^2] \qquad (4)$$

Which can be rewritten in the form:

$$1/(n^2-1)=(E_{so}/E_d)+[(1/E_dE_{so})/(h\nu)^2] \qquad (5)$$

Where E_d is the oscillator strength or dispersion energy and E_{so} is the single oscillator energy or average energy gap. Factor E_d which is the mean energy of transition of the lone-pair state to the conduction band state depends on the imaginary part of dielectric constant (ε_i) whereas E_{so} does not. Due to this reason E_d is very nearly independent of E_{so}, and E_{so} is related to the bond energy of chemical bonds present in the system. For oscillator parameters to be calculated a graph of $(n^2\text{-}1)^{-1}$ and $(h\nu)^2$ is drawn (Fig. 4-i) and the linear portion of the curve were up to the proximity of the band edge, where such a linear fit is valid near the optical energy gap is fitted to a straight line with a slope $-1/E_{so}E_d$ and an intercept E_{so}/E_d as depicted in Fig. 4-ii. The dispersion parameters E_d and E_{so} are calculated and listed in Table 2. E_{so} is considered a good approximation to an average energy gap; it varies in proportion to the Tauc band-gap E_g: $E_{so}\approx 2E_g$ [11]. The dispersion plays a significant role with respect to optical communication and spectral dispersion [12].

The moments of optical dispersion spectra M_{-1}, and M_{-3}, can be evaluated using the relationships [13]:

$$E_{so}^2=\frac{M_{-1}}{M_{-3}} \quad and \quad E_d^2=\frac{M_{-1}^3}{M_{-3}} \qquad (6)$$

The zero-frequency refractive index (static refractive index) is obtained using (4), by putting hν=0, i.e. based on the expression:

$$n_o^2-1=\frac{E_d}{E_{so}} \qquad (7)$$

The values of static refractive index n_o are calculated and recorded in Table. 2. The values of dispersion parameters and the optical moments gathered in Table 2., are strongly agree with Wemple [9] and DiDomenico [10].

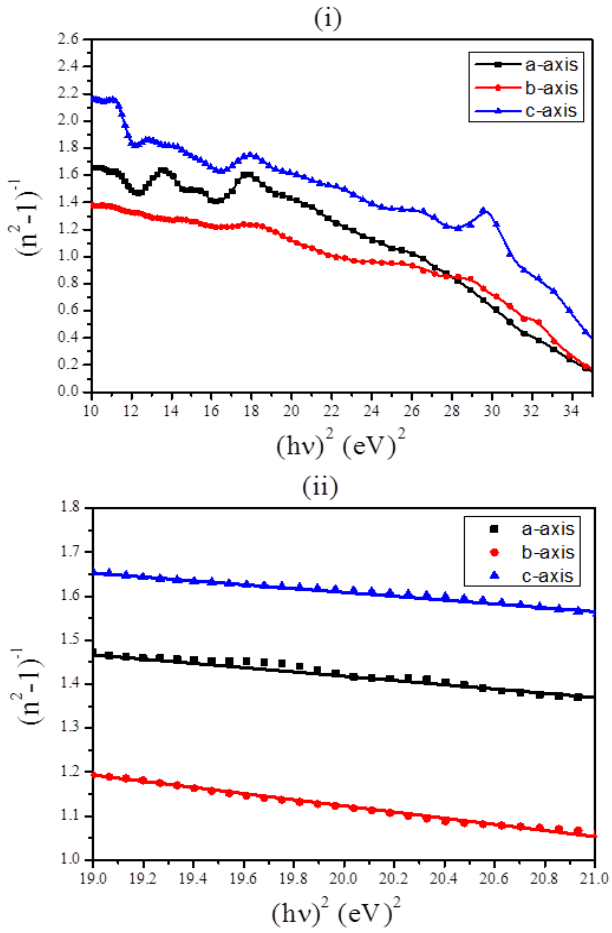

Fig. 4. (i) Plot of $(n^2\text{-}1)^{-1}$ versus $(h\nu)^2$, (ii) the best fit of $(n^2\text{-}1)^{-1}$ versus $(h\nu)^2$ around the energy gap with respect to the principle crystallographic axes of $KHSeO_4$ single crystal.

TABLE 2. NORMAL DISPERSION PARAMETERS FOR $KHSeO_4$ SINGLE CRYSTAL.

Physical quantity	Value		
	a-axis	b-axis	c-axis
Optical energy gap E_g (eV)	4.559	4.486	4.580
Refractive index n	1.3141	1.3779	1.2802
Extinction coefficient k.	4.5732×10^{-5}	4.2432×10^{-5}	2.9054×10^{-5}
Single oscillator energy E_{so} (eV)	6.7966	6.0313	7.6644
Dispersion energy E_d (eV)	2.7086	2.4205	3.1371
Moment of the optical dispersion spectra M_{-1} $(eV)^2$	0.3985	0.4013	0.4093
Moment of the optical dispersion spectra M_{-3} $(eV)^{-2}$	8.6272×10^{-3}	11.0322×10^{-3}	6.9677×10^{-3}
Static refractive index no	1.1826	1.1838	1.1871

The dispersion of the refractive indexes in anisotropic $KHSeO_4$ single crystals is refined. It is found that values of the refractive indexes depend on the crystal axes and also depend on the radiation energy. This dependence is very important in using crystals as working elements of optical and quantum electronic devices.

3.6. Optical constants

The dielectric constant ε can be expressed as a complex equation in the form $\varepsilon=\varepsilon_r - i\varepsilon_i$, where ε_r is the real part generally relates to dispersion, while ε_i is the imaginary part provides a measure of the dissipative rate of the wave in the medium. The real and imaginary parts of the complex dielectric constant are related to the refractive index and the extinction coefficient as:

$$\varepsilon_r = n^2 - k^2 \quad and \quad \varepsilon_i = 2nk \tag{8}$$

It is clear from (8), that the variation of ε_r follows the same trend as refractive index (n) on photon energy hν, whereas the variation of ε_i mainly follows the behavior of the extinction coefficient k and the absorption coefficient (α) is the same as shown in Fig. 5.

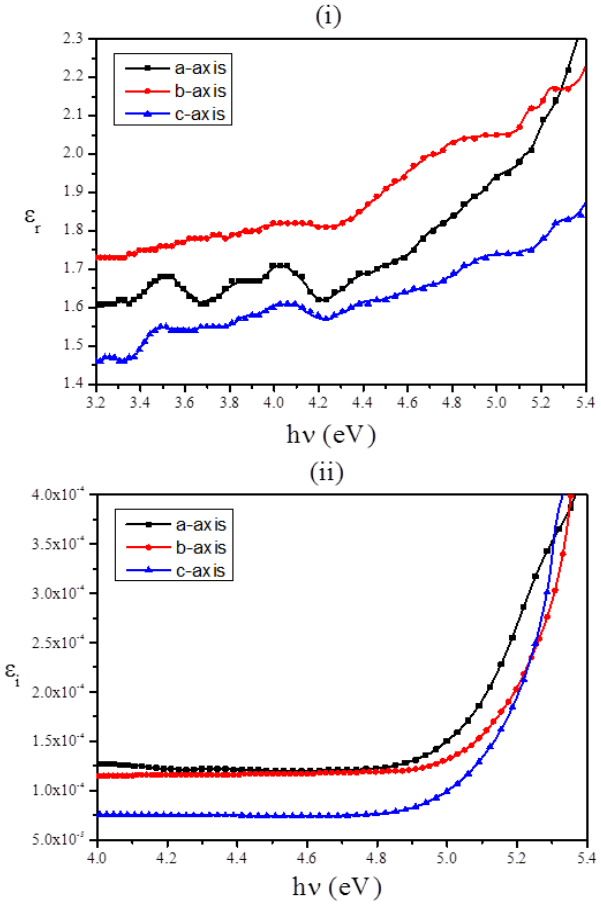

Fig. 5. The spectral behaviour of (i) real ε_r , and (ii) imaginary ε_i, parts of the dielectric constant with respect to the principle crystallographic axes of $KHSeO_4$ single crystal.

The optical conductivity is a measure of the frequency response of the material when irradiated with light and related to electrical conductivity by the following equations [14]:

$$\sigma_{opt.} = \frac{nck}{\lambda} \quad and \quad \sigma_{ele.} = \frac{\lambda^2}{2\pi k}\sigma_{opt.} \tag{9}$$

Where λ is the incident wavelength and c is the velocity of light. The energy dependence of the optical and electrical conductivities is illustrated in Fig. 6. It can be seen from the figure that the optical conductivity $\sigma_{opt.}$ increases with increasing the incident photon energy while the electrical conductivity $\sigma_{ele.}$ takes the opposite behavior in the same photon energy range.

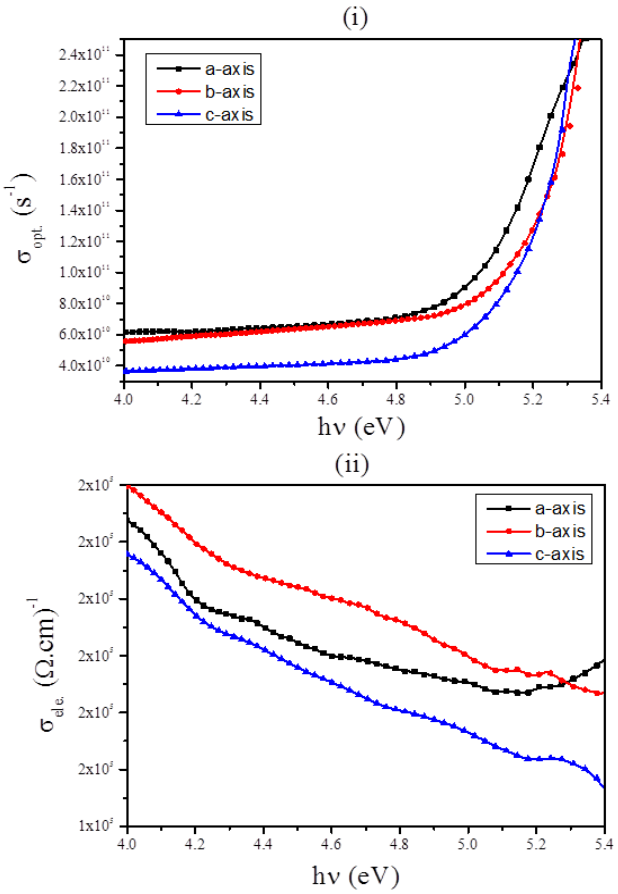

Fig. 6. The spectral behavior of (i) optical $\sigma_{opt.}$ and (ii) electrical $\sigma_{ele.}$ conductivities measured in the direction of the principle crystallographic axes of $KHSeO_4$ single crystal.

The spectra of the optical conductivity $\sigma_{opt.}$ and the imaginary part of the dielectric constant ε_i measured in the a- and b-axes exhibit a convergence near the value of the energy gap. This convergence results from that (8) and (9) depend on k and n with neither of them being the dominant term that resulted in a behavior in middle between the n and k spectra.

Lattice dielectric constant ε_L and contribution of charge carriers (*N*) can be calculated by the fitting of the linear part of the relation [15]:

$$n^2 = \varepsilon_L - \left(\frac{N}{m^*}\right)\left(\frac{e^2h^2}{4\pi^2\varepsilon_o}\right)\frac{1}{\lambda^2} \tag{10}$$

Where e is electronic charge, c is the velocity of light and N/m^* is the ratio of carrier concentration to effective mass; Fig. 7-ii shows the fitting of equation (10). The relation shows

that when the carrier concentration increases the energy gap decreases and so the refractive index increases.

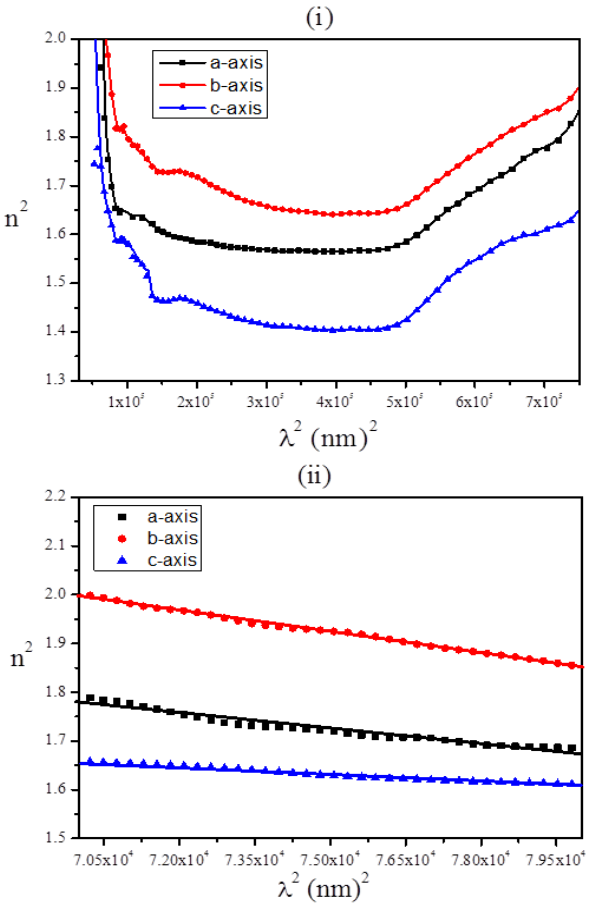

Fig. 7. (i) Plot of n^2 versus λ^2, (ii) the best fit of n^2 versus λ^2 around the energy gap with respect to the principle crystallographic axes of $KHSeO_4$ single crystal.

The electric susceptibility χ_c can be calculated from the optical measurements according to the relation [16]:

$$\varepsilon_r = \varepsilon_o + 4\pi\chi_c = n^2 - k^2 \qquad (11)$$

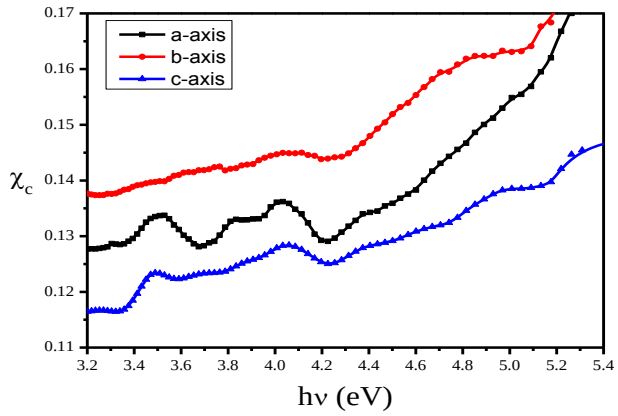

$$\chi_c = \frac{(n^2 - k^2 - \varepsilon_o)}{4\pi} \qquad (12)$$

Fig. 8. The spectral behavior of the electric susceptibility χ_c in the principle crystallographic axes of $KHSeO_4$ single crystal.

TABLE 3. OPTICAL PARAMETERS FOR $KHSeO_4$ CRYSTAL IN THE PRINCIPLE CRYSTALLOGRAPHIC DIRECTIONS.

Physical quantity	Value		
	a-axis	b-axis	c-axis
Optical conductivity $\sigma_{opt.}$ (s^{-1})	6.6161×10^{10}	6.3321×10^{10}	4.1099×10^{10}
Electrical conductivity $\sigma_{ele.}$ $(\Omega.cm)^{-1}$	1.7097×10^{5}	1.8223×10^{5}	1.65951×10^{5}
Electric susceptibility χ_c	0.1374	0.1511	0.1304
Lattice dielectric constant ε_L	2.5095	3.004	2.0198
The ratio of carrier concentration to effective mass N/m^* $(m^3.kg)^{-1}$	1.2815×10^{58}	1.7634×10^{58}	6.33×10^{58}

CONCLUSIONS

1- Good quality, highly transparent and well faceted large size single crystals of $KHSeO_4$ were grown by solution growth technique.

2- FTIR spectra were measured for the as grown and annealed crystals and the functional groups were assigned. For annealed samples, some absorption peaks decrease or increase in intensities. There is a transformation of some sharp peaks to broad humps.

3- From the data of the absorption coefficient (α) the optical band gap E_g was deduced in the three crystallographic directions for samples of $KHSeO_4$ single crystal. The type of transition was allowed indirect one.

4- The refractive index (n) values are calculated as a function of photon energy. The refractive index values have been fitted to the single oscillator Wemple–DiDomenico (WDD) model. And the dispersion parameters were calculated in the normal dispersion region around the optical energy gap for the three crystallographic directions.

5- Values of the extinction coefficient (k), the real and imaginary parts (of the dielectric constant and the optical and electrical conductivities ($\sigma_{opt.}$ & $\sigma_{ele.}$) were estimated for $KHSeO_4$ crystal along the principal crystallographic axes. The high magnitude of optical conductivity and the low extinction coefficient (10^{-5}) confirms the presence of very high photo response nature of the material. This makes the material more prominent for device applications of various optoelectronics and photonic devices.

6- The calculated optical constants for $KHSeO_4$ crystals clearly depend on the direction of crystallographic axis which confirms their anisotropic character.

REFERENCES

[1] S.M. Haile, D.A. Boysen, C.R.I. Chisholm, and R.B. Merle, "Solid acids as fuel cell electrolytes", Nature, vol. 410, pp. 910–913, April 2001. doi:10.1038/35073536

[2] Z. Czapla, T. Lis and L. Sobczyk, "Ferroelectric properties of NH_4HSeO_4 crystals", Phys. Stat. Sol. (a), vol. 51, pp. 609–612, February 1979. doi: 10.1002/pssa.2210510237

[3] J. Baran and T. Lis, "Structure of potassium hydrogenselenate", Acta Cryst. C, vol. 42, pp. 270–272, March 1986. doi:10.1107/S010827018609652X

[4] T. S. Moss, G. J. Burrel and E. Ellis, "Semiconductor Opto-electronics", Butterworths, London, 1973.

[5] A. Goypiron, J. De Villepin and A. Novak, "Raman and infrared study of $KHSO_4$ crystal", J. Raman Spectrosc., vol. 9, pp. 297–303, October 1980. doi: 10.1002/jrs.1250090505

[6] J. Baran, "Polarized infrared spectra of $KHSeO_4$ single crystal", Spectrochim. Acta (A), vol. 42, pp. 1365–1371, June 1986. doi:10.1016/0584-8539(86)80246-X

[7] J. Tauc, R. Grigorovici and A. Vancu, "Optical properties and electronic structure of amorphous Germanium", Phys. Stat. Sol. (b), vol. 15, pp. 627–637, March 1966. doi:10.1002/pssb.19660150224

[8] A. Abu El-Fadl, M.A. Gaffar and M.H. Omar, "Absorption Spectra and Optical Parameters of Lithium-Potassium Sulphate Single Crystals", Physica B, vol. 269, pp. 403–408, December 1999. doi:10.1016/S0921-4526(99)00117-9

[9] S. H. Wemple, M. DiDomenico and Jr., "Behavior of the Electronic Dielectric Constant in Covalent and Ionic Materials", Phys. Rev. B, vol. 3, pp. 1338–1351, Februry 1971.doi:10.1103/PhysRevB.3.1338

[10] S.H. Wemple and M. DiDomenico, "Optical Dispersion and the Structure of Solids", Phys. Rev. Lett., vol. 23, pp. 1156–1159, November 1969. doi: 10.1103/PhysRevLett.23.1156

[11] K. Tanaka, "Optical properties and photoinduced changes in amorphous As_xS_{100-x} films", Thin Solid Films, vol. 66, pp. 271–279, July 1980. doi:10.1016/0040-6090(80)90381-8

[12] M. Fadel, S.A. Fayek, M.O. Abou-Helal, M.M. Ibrahim and A.M. Shakra, "Structural and optical properties of SeGe and SeGeX (X = In, Sb and Bi) amorphous films", J. Alloys Compd., vol. 485, pp. 604–609, June 2009. doi:10.1016/j.jallcom.2009.06.057

[13] Y. Caglara, S. Ilican and M. Caglar, "Single-oscillator model and determination of optical constants of spray pyrolyzed amorphous SnO_2 thin films", Eur. Phys. J. B, vol. 58, pp. 251–256, September 2007. doi:10.1140/epjb/e2007-00227-y

[14] T. C. Sabari Girisun and S. Dhanuskodi, "Linear and nonlinear optical properties of tris thiourea zinc sulphate single crystals", Cryst. Res. Technol., vol. 44, pp. 1297–1302, December 2009. doi:10.1002/crat.200900351

[15] A. Dahshan, H.H. Amer and K.A. Aly, "Compositional dependence of the optical constants of amorphous $Ge_xAs_{20}Se_{80-x}$ thin films", J. Phys. D: Appl. Phys., vol. 41, pp. 215401, November 2008. doi:10.1088/0022-3727/41/21/215401

[16] V. Gupta and A. Mansingh, "Influence of post deposition annealing on the structural and optical properties of sputtered zinc oxide film", J. Appl. Phys., vol. 80, pp. 1063–1073, March 1996. doi:10.1063/1.362842